Journal of Alloys and Compounds 695 (2017) 3018–3023

Contents lists available at ScienceDirect

Journal of Alloys and Compounds

journal homepage: http://www.elsevier.com/locate/jalcom

Lanthanide ions-doped calcium molybdate pie-like microstructures: Synthesis, structure characterization, and luminescent properties

Yuanyuan Han [b, **], Liyong Wang [a, *], Dan Wang [a], Danyang Liang [a], Shiqi Wang [a], Guoxin Lu [a], Zhiyu Di [a], Guang Jia [a]

[a] College of Chemistry and Environmental Science, Key Laboratory of Medicine Chemistry and Molecular Diagnosis, Ministry of Education, Hebei University, No. 180 Wusi Road, Baoding 071002, PR China
[b] Medical Experimental Centre of Hebei University, No. 342 Yuhua Road, Baoding 071000, PR China

ARTICLE INFO

Article history:
Received 10 September 2016
Received in revised form
16 November 2016
Accepted 24 November 2016
Available online 25 November 2016

Keywords:
Calcium molybdate
Hydrothermal synthesis
Phenol-formaldehyde resin
Lanthanide ions
Luminescence properties

ABSTRACT

Lanthanide ions doped $CaMoO_4$ with pie-like microstructures were synthesized by a hydrothermal method using phenol-formaldehyde resin (PF) as an inducer. The results of powder X-ray diffraction showed a tetragonal phase of both undoped and Ln^{3+}-doped $CaMoO_4$. The microscopical characterization technology revealed the formation process of the pie-like microparticles. As a morphology inducer, the PF molecules played an important role in the formation of phase structure. The as-obtained materials were characterized using different spectroscopic techniques including FT-IR, Raman spectrum, and PL. The emission color can be easily turned by adjusting the relative doping concentrations of lanthanide ions.

1. Introduction

Nowadays, great attention has been paid for the synthesis of lanthanide ion (Ln^{3+}) doped nano/micrometer particles due to their wide applications such as in optoelectronic and biological field [1–7]. The unique morphologies with self-assembled hierarchical superstructures also provide subtle complex functions and direct bridges between the microscale objects and the macroscale world [8,9]. Calcium molybdate ($CaMoO_4$), as a famous host material with scheelite structure has been widely studied in scintillators, X-ray phosphors, laser crystals, and host lattices in electron spin resonance due to its excellent optical properties [10–14].

Lanthanide ions doped $CaMoO_4$ nano or micrometer particles have been prepared by various synthetic methods by previous reports [15–20]. The results revealed the relations between particles size or hierarchical morphology and luminescent properties.

Herein, for the first time we report the controllable fabrication of novel lanthanide ions doped $CaMoO_4$ hierarchical architectures with good uniformity *via* a facile hydrothermal method. PF molecules were used as a shape inducer in hydrothermal condition. In addition, the possible formation mechanism of the pie-like microstructure is proposed. Compared to the previously reports, our method has advantages including cheap chemical reagents, facile synthetic procedure, and relatively low reaction temperature. The phase structure, IR, Raman, and PL spectra, and chromatic properties were also investigated.

2. Experimentals

2.1. Synthesis

All the chemical reagents were of analytical grade and used as received without further purification.

A low temperature hydrothermal method was used to synthesize the micrometer pie-like $CaMoO_4$ particles. In a typical synthesis process, $Ca(NO_3)_2$ (5.0 mmol) and different types and amounts of $Ln(NO_3)_3$ (Tb^{3+}, Dy^{3+}, and Eu^{3+}) were dissolved in 15 mL of distilled water. Then, the mixed solution was dropped into 15 mL of Na_2MoO_4 (5.0 mmol) solution slowly under vigorous stirring. Afterwards, phenol, formaldehyde and ammonia water (13.33 mol L^{-1}) was added into the above solution. After continuous

* Corresponding author.
** Corresponding author.
E-mail addresses: hanyy_8016@163.com (Y. Han), wangly_1@126.com (L. Wang).

http://dx.doi.org/10.1016/j.jallcom.2016.11.355
0925-8388/

stirring of 5 min, the precursor suspension was transferred into a 50 mL Teflon-lined stainless steel autoclave with a filling capacity of 75%, which was subsequently sealed and heated to 160 °C for 4 h. Then the autoclave was cooled to room temperature naturally. After the centrifugation of the resulting solutions, the products were washed several times with deionized water and ethanol, then air dried at 100 °C overnight. Then the product was calcinated at 600 °C to remove the PF polymer, followed by grinding to yield the final lanthanide ions doped $CaMoO_4$ powder.

2.2. Characterization

The crystallinity and phase purity of $CaMoO_4$ samples were examined by powder X-ray diffraction (XRD) with an X-ray diffractometer (D8 ADVANCE, Bruker, USA) with graphite monochromatic Cu Ka radiation. The morphology and size of the as-synthesized products were investigated using a scanning electron microscope (SEM, JEOL, JSM-7500F, Japan). The FT-IR spectroscopy (IR, Perkin-Elmer, 580B, USA) was performed to confirm the surface chemical structure of the products in the wave number range of 400–4000 cm^{-1} by KBr disk method. Thermogravimetric analysis (TGA) and Differential Thermal Analysis (DTA) was carried out on a Simultaneous Thermal Analyzer (Netzsch, STA 449c, Germany) with a heating rate of 10 °C/min from 50 to 800 °C under air atmosphere. Characteristic vibration energy changing of chemical bond and group were recorded on a Laser Raman microscope equipment (Xplora, Horiba, France). The photo-luminescent (PL) excitation and emission spectra were recorded with spectrophotometer (PL, Hitachi, F-7000, Japan). The chromaticity coordinates calculated by the CIE system.

3. Results and discussion

The XRD patterns of $CaMoO_4$:xDy^{3+} (0–0.10) phosphors are shown in Fig. 1a. It shows that all the diffraction peaks match well with the tetragonal phase of $CaMoO_4$ according to the standard reference of JCPDS card no. 41-1431, no additional peaks for impurity phases are observed, indicating that the Dy^{3+} ions can be effectively doped into the $CaMoO_4$ host and the dopants do not cause any significant changes to the host structure. However, the diffraction peak for (112) plane shifts to higher angles for Dy^{3+} ion substitution, suggesting the decrease of the lattice constants by doping Dy^{3+} ions [21]. PF polymer template can also affect the crystal structure. From Fig. 1b, it can be observed that different amount of phenol adding influences the formation of crystal structure. Comparing with that of the sample prepared in the absence of phenol, the main diffraction peaks shift to higher angles.

As it is known that the surface chemistry properties and template of the materials can be examined by FTIR spectra. Fig. 2 presents the FTIR spectra of the as-synthesized products, and Fig. 2a represents the PF template synthesized by hydrothermal condition. The absorption band composition is consistent with that of PF reported previously [22,23], such as vibrations of the carboxylate groups (1632 cm^{-1}), absorption bands of the benzene rings (1612, 1479 cm^{-1}), the C–H outer bending vibrations (1146 cm^{-1}), absorption of CH_2 groups (966, 826 cm^{-1}), absorption of phenolic OH in-plane deformation (1357 cm^{-1}), absorption of alkyl-phenol C–O stretch (1229 cm^{-1}) and CH_2 out of plane ring deformation (802 cm^{-1}). Furthermore, Fig. 2b represents PF/$CaMoO_4$ compound without calcination process. Besides the characteristic peaks of PF, it can be also observed that characteristic absorption band Mo–O at 820, 435 cm^{-1} for stretching and bending mode respectively, which

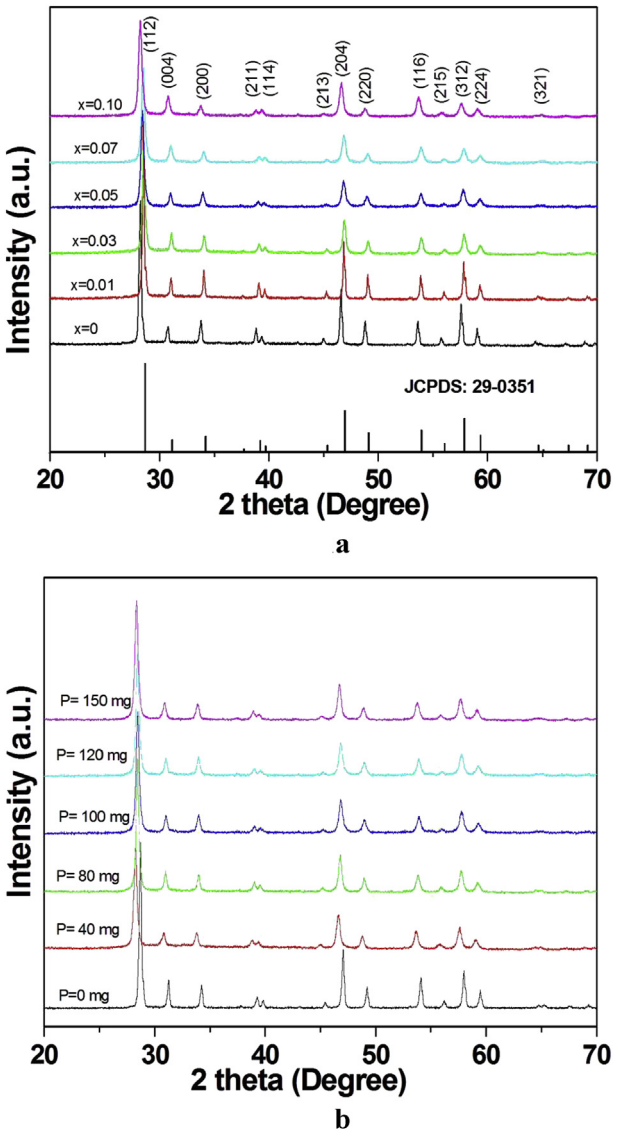

Fig. 1. a). XRD patterns of $CaMoO_4$ samples doped with different amount of Dy^{3+}. (b). XRD patterns of lanthanide ions doped $CaMoO_4$ (5 at. %) samples obtained with different amount of PF precursor.

confirms the presence of the composite structure. Eventually, Fig. 2c shows the as-prepared product after 600 °C calcination, the absence of the characteristic absorption bands indicates that no polymer template remaining after calcination process.

The thermal behaviors of the as-prepared hydrothermal product before calcination were investigated by TG-DTA measurements (Fig. 3). There is one sharp weight loss in the TG curve accompanying two exothermic peaks in the range of 300–600 °C, which can be can be assigned to the dehydration and decomposition of PF. It can also be seen that the mass of compound is stable when the calcination temperature is higher than 600 °C, resulting in the pure $CaMoO_4$ product.

The structure order of material at short range and the Raman-active phonon modes can be measured by the FT-Raman technology at room temperature. It is known that 13 modes are Raman active ($3A_g$, $5B_g$, $5E_g$) and 8 mode are IR active among 26 modes of vibrations ($3A_g$, $5A_u$, $5B_g$, $3B_u$, $5E_g$, $5E_u$) for Scheelite structure

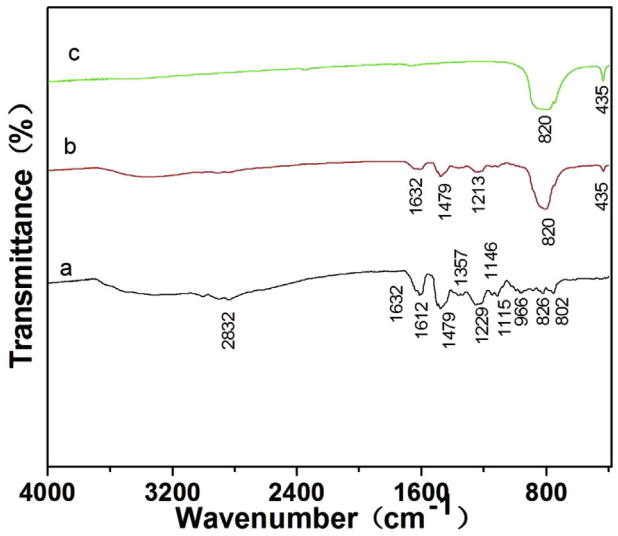

Fig. 2. FTIR spectra of the PF template, as-prepared and 600 °C calcinated $CaMoO_4$ samples (a: PF, b: $CaMoO_4$/PF, c: $CaMoO_4$).

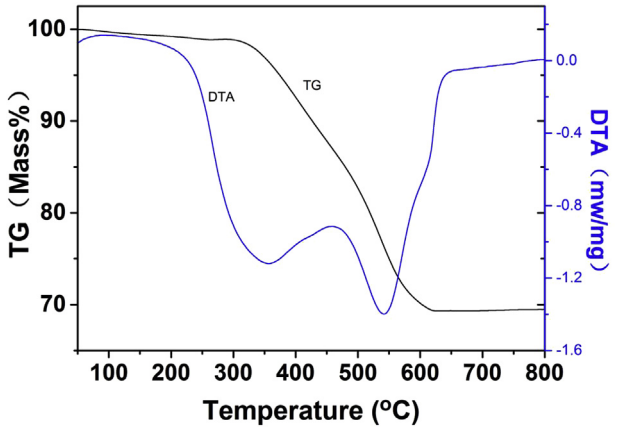

Fig. 3. TG/DTA isotherms of compound of 5 at% doped $CaMoO_4$:Dy^{3+} and PF before calcination process.

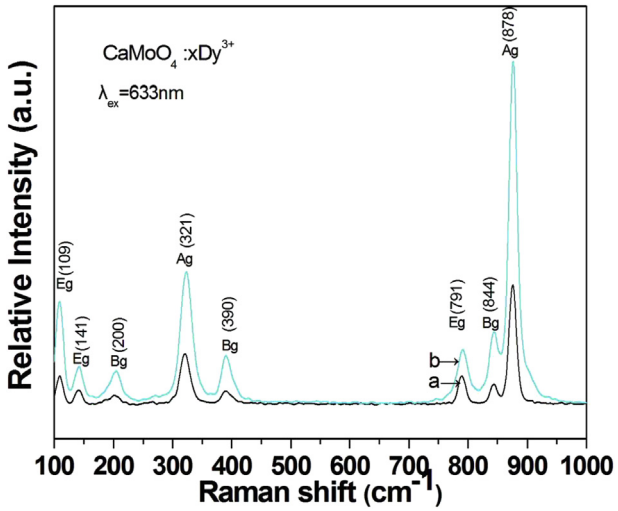

Fig. 4. FT-Raman spectra of the as-prepared $CaMoO_4$: xDy^{3+} (a) x = 0%, (b) x = 5% pie-like microparticles.

[24–26]. Fig. 4 presents the Raman spectra of the as-synthesized $CaMoO_4$ and Dy^{3+} ions doped $CaMoO_4$ (7%), it can be observed that both Raman spectra exhibit intense and sharp band due to strong interaction between the O–Ca–O and O–Mo–O in the $CaMoO_4$ matrix. The strong intense bands at 878, 844, and 791 cm^{-1} are due to A_g, B_g, and E_g modes, furthermore, the bands at 109, 141, 200, 321, and 390 cm^{-1} are due to E_g, E_g, B_g, $A_g + E_g$ and A_g modes. It can be observed that Dy^{3+} doping did not generate obvious changing for Raman spectra except band intensity, it may be ascribe to local disorder and defects in the scheelite lattice of $CaMoO_4$ after doping of Dy^{3+}. Since Mo^{6+} ion located at the site B in the $CaMoO_4$ matrix, the replacement of Ca^{2+} ions by Dy^{3+} ions at site A, which can barely impact the atom arrangement after doping. Therefore, Dy^{3+} doping cannot modify stretching, torsion, and bending vibration modes of Mo–O bonds [27].

The effect of reaction time on the morphology evolution of the $CaMoO_4$:Dy^{3+} microstructure was investigated in detail at 160 °C for a given time. Fig. 5a–d shows SEM images of $CaMoO_4$:Dy^{3+} prepared with different reaction time and the polymer precursors were 100 mg phenol, 0.3 mL ammonium hydroxide (25%), and 0.2 mL formaldehyde. And it can be observed that when the hydrothermal reaction proceeded for 0.5 h, the product was mainly composed of regular nanospheres with a typical diameter rang of 100–150 nm, and most of the nanospheres have obvious boundary and narrow particle size distribution. However, some of them are interconnecting together and merge into larger particles. When the reaction time increased to 1 h, larger nano-rods were formed *via* the Ostwald ripening mechanism to form three-dimensional microspheres through oriented-attachment and self-assembly [28,29]. As the reaction time was extended to 2 h, the morphology and size of microspheres were relatively uniform compared to those of the products processed for 1 h, and the pie-like morphology appeared with rough surfaces. With the increase of reaction time to 4 h, the micro-pies had little changes in thickness and length but with a uniform morphology. Furthermore, the polymer additive was also an important controlling factor in shaping the product. It can be observed that (from Fig. 4e) the irregular morphology appeared when the polymer precursor was excessively surplus.

The whole evolution process for the as-prepared pie-like $CaMoO_4$ hierarchical structures is thereby illustrated in Fig. 6.

Fig. 6 shows the schematic illustration of the possible formation process for the $CaMoO_4$ samples. $CaMoO_4$ nanocrystals were immediately formed after blending of Ca^{2+} with MoO_4^{2-} ions. The mixed solution of ammonia water, formaldehyde, and phenol could be the precursor of PF (phenol formaldehyde resin) under hydrothermal condition. PF coated on $CaMoO_4$ nanocrystals may act as anti-growing and assembling agent, thus the compound of polymer/$CaMoO_4$ showed uniform particles size and narrow distribution. After the thermal decomposition of PF molecules into small inorganic molecules such as NO_x, H_2O and CO_2 in calcination process, the pure micrometer pie-like $CaMoO_4$ was subsequently obtained.

Fig. 7 shows the excitation spectra of Dy^{3+} (5 at. %) doped $CaMoO_4$ by monitoring the emission wavelength at 573 nm. It can be observed that a broad band with a maximum at 274 nm due to the MoO_4^{2-} groups from 225 to 320 nm. Meanwhile, some weak lines due to the f–f transitions of Dy^{3+} can be observed in the wavelength ranging of 350–450 nm. And these weak lines at 352, 366, 388, 399, 428, and 450 nm are assigned to the transitions from the $^6H_{15/2}$ ground state to the different excited states of Dy^{3+}, i. e., $^6F_{7/2}$ (352), $^6F_{9/2}$ (366), $^4I_{13/2}$ (388), $^4F_{7/2}$ (399), $^4G_{11/2}$ (428), and $^4I_{15/2}$ (450), respectively. These were assigned to the combination of the ligand to metal charge transfer (O^{2-}/Mo^{6+}) and charge transfer band (CTB) from the completely filled 2p orbitals of O^{2-} to the

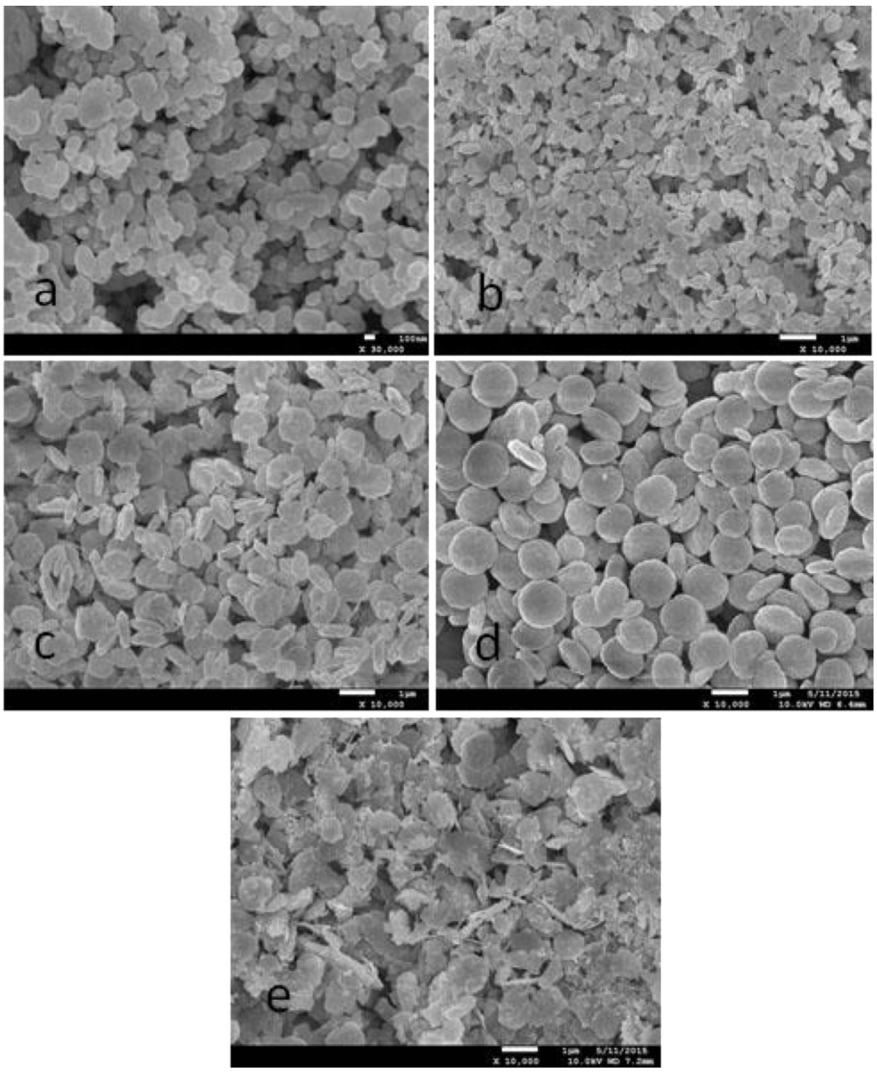

Fig. 5. SEM images of the as-prepared $CaMoO_4$ with different hydrothermal reaction time (a: 0.5 h, b: 1 h, c: 2 h, and d: 4 h) and e (redundant polymer additive).

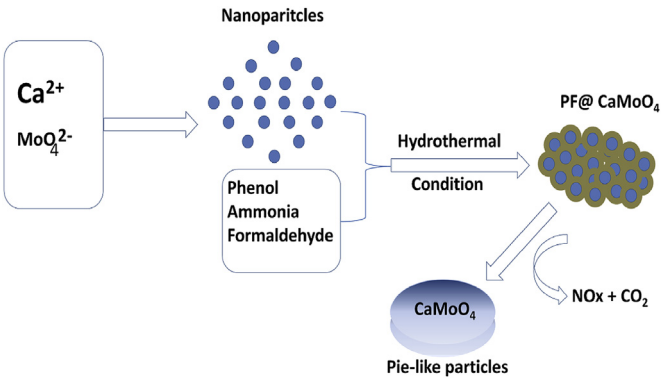

Fig. 6. Schematic illustration of the possible formation process.

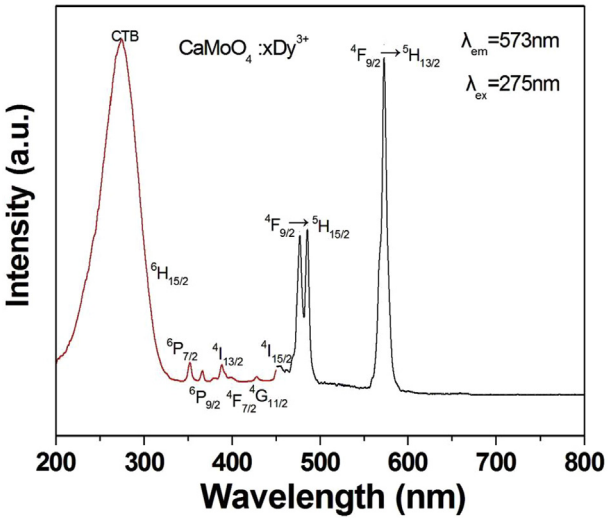

Fig. 7. Excitation and emission spectra of $CaMoO_4$:xDy^{3+} (x = 5 at. %) microparticles.

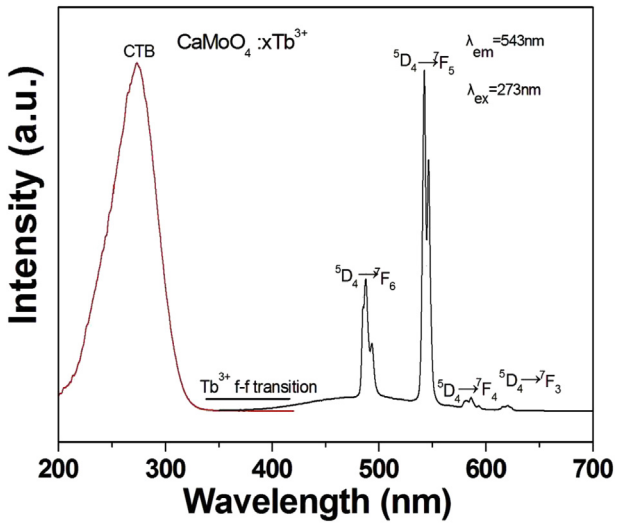

Fig. 8. Excitation and emission spectra of $CaMoO_4$:xTb^{3+} (x = 5 at. %) microparticles.

partially filled f–f orbitals of the Dy^{3+} ions (O^{2-}/Dy^{3+}) [10]. In the emission spectra, the transition band at $^4F_{9/2}$–$^6H_{15/2}$ (487 nm) is assigned to the magnetic dipole transition, whereas that at $^4F_{9/2}$–$^6H_{13/2}$ (573 nm) assigns to electric dipole transition [10]. The yellow luminescence color is dominated by the transition at $^4F_{9/2}$–$^6H_{13/2}$ (573 nm) in all the cases.

Fig. 8 shows the excitation and emission spectra of $CaMoO_4$:Tb^{3+}. It can be observed that a strong and broad band from 200 to 320 nm with a maximum at about 273 nm is assign to the charge-transfer transitions within the MoO_4^{2-} groups. In the wavelength ranging from 320 to 420 nm, the weak lines ascribed to the f-f transitions within the Tb^{3+} $4f^8$ configuration can be hardly detected because of their weak intensity. Upon excitation into the MoO_4^{2-} at 273 nm, the emission spectrum contains the characteristic emission of Tb^{3+} with $^5D_4$–$^7F_5$ green emission (543 nm) as the most prominent group. Other emissions are located at 488, 586, and 621 nm, which can be ascribed to the transitions of $^5D_4$–$^7F_6$, $^5D_4$–$7F_4$, and $^5D_4$–$^7F_3$, respectively [30].

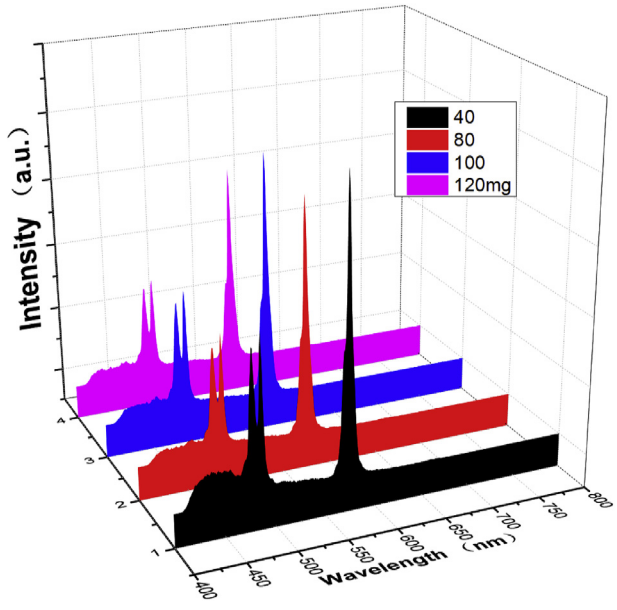

Fig. 9. Emission spectra of $CaMoO_4$:xTb^{3+} (x = 5 at. %) microparticles with different amount of phenol.

Fig. 9 shows the emission spectra of $CaMoO_4$:xTb^{3+} (x = 5%) microparticles with different amount of phenol. It can be seen that the fluorescence intensities change slightly, therefore, PF precursors formation in hydrothermal condition and degradation during calcination process have little effect on the fluorescence emission.

The tunable emission properties of the $CaMoO_4$ phosphors can be investigated by co-doping different lanthanide ions. Fig. 10 a and b show the emission spectra of the co-doped $CaMoO_4$ with different relative concentrations of Dy^{3+}, Eu^{3+}, and Tb^{3+} (total concentration: 5 at. %) under excitation at 273 nm, respectively. It can be seen that the as-obtained lanthanide ions co-doped $CaMoO_4$ phosphors showed strong different emissions. When Eu^{3+} ions were co-doped into the $CaMoO_4$ host lattices, besides the Dy^{3+} emissions the characteristic emissions of the Eu^{3+} could be also observed. Moreover, the emission intensity of Dy^{3+} decreased gradually by increasing the relative concentration ratio of Eu^{3+}. It can be also seen that the emission colors can be turned from green, through yellow or yellow-red, to red by adjusting the relative doping concentrations of the Tb^{3+} and Eu^{3+} ions (Fig. 10b). The result indicates that the pie-like phosphors show multicolor emissions when excited under UV light, which makes them act as potential phosphors for light powders and advanced flat panel display devices [31].

The $CaMoO_4$:Ln^{3+} (Ln = Eu, Tb, and Dy) samples exhibit intense characteristic emissions of lanthanide activator ions under UV excitation, which can be confirmed by the CIE (Commission Internationale de l'Eclairage 1931 chromaticity) coordinates for the emission spectra of the $CaMoO_4$:Ln^{3+} samples (Fig. 11). The chromaticity coordinates of $CaMoO_4$:Ln^{3+} (Ln = Eu^{3+}, Tb^{3+}, and Dy^{3+}) samples are calculated to be x = 0.397, y = 0.318 (point a); x = 0.217, y = 0.453 (point b); x = 0.344, y = 0.414 (point c). It can be observed that the PL emission colors of the $CaMoO_4$:Ln^{3+} samples can be tuned by doping different lanthanide activator ions.

4. Conclusion

In summary, the novel pie-like architectures of lanthanide ions doped $CaMoO_4$ phosphors have been successfully prepared *via* a facile and efficient hydrothermal process by controlling the fundamental experimental parameters. The amount of PF precursor played a key role in the formation of $CaMoO_4$ microstructure, and the formation mechanism of the structure has been investigated in detail. Furthermore, the emission colors can be turned easily by adjusting the relative doping concentrations of lanthanide ions. The as-obtained uniform and well-dispersed $CaMoO_4$:Ln^{3+} phosphors exhibit strong emission, which may find great potential applications in lighting, displays, and devices in photochemical fields. Furthermore, this facile strategy described here may serve as guidance for the design of new well-defined molybdate materials.

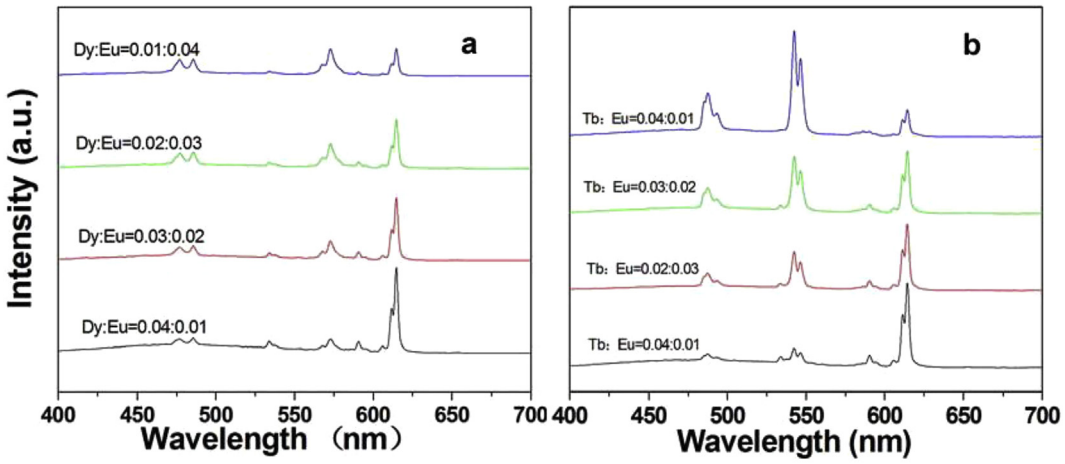

Fig. 10. Emission spectra of the $CaMoO_4$ co-doped with Dy^{3+}/Eu^{3+} (a) and (b) co-doped with Tb^{3+}/Eu^{3+}.

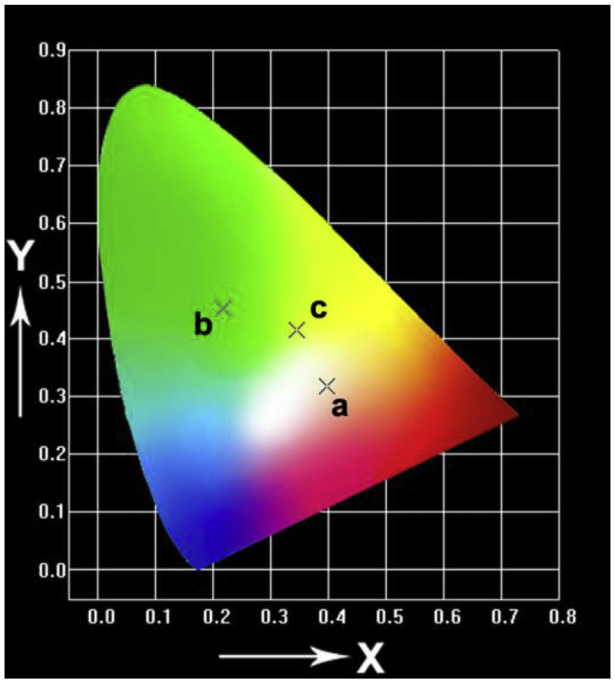

Fig. 11. CIE chromaticity diagram of $CaMoO_4:Ln^{3+}$ (5 at. %) samples: (a) Eu^{3+}, (b) Tb^{3+} and (c) Dy^{3+}.

Conflict of interest

The authors declare that they have no conflict of interest.

Acknowledgments

This study was funded by Project of Medical disciplines construction funds of Hebei University (Grant No. 2015A2004), project of Hebei education department (Grant No. Z2013053) Students Research Fund of College of Chemistry and Environmental Science (Grant No. 2015010), Natural Science Foundation of Hebei University (Grant No. 2013-254), the Second Batch of Top Youth Talent Support Program of Hebei Province.

References

[1] M. Antonietti, G.A. Ozin, Chem. Eur. J. 10 (2004) 28–41.
[2] J.J. Feng, Q.C. Liao, A.J. Wang, J.R. Chen, CrystEngComm 13 (2011) 4202–4210.
[3] B. Liu, S.H. Yu, L. Li, Q. Zhang, F. Zhang, K. Jiang, Angew. Chem. Int. Ed. 43 (2004) 4745–4750.
[4] P. Ghosh, J. Oliva, E.D. Rosa, K.K. Haldar, D. Solis, A. Patra, J. Phys. Chem. C 112 (2008) 9650–9658.
[5] A. Kar, A. Datta, A. Patra, J. Mater. Chem. 20 (2010) 916–922.
[6] A.K. Parchur, R.S. Ningthoujam, Dalton Trans. 40 (2011) 7590–7594.
[7] A.A. Ansari, M. Alam, J.P. Labis, S.A. Alrokayan, G. Shafi, T.N. Hasan, N.A. Syed, A.A. Alshatwi, J. Mater. Chem. 21 (2011) 19310–19316.
[8] X.G. Liu, L. Li, H.M. Noh, S.H. Park, J.H. Jeong, H.K. Yang, K. Jang, D.S. Shin, Opt. Mater. 43 (2015) 10–17.
[9] S. Mann, Angew. Chem. Int. Ed. 39 (2000) 3392–3406.
[10] K. Gayatri Sharma, N. Rajmuhon Singh, New J. Chem. 37 (2013) 2784–2791.
[11] J.S. Thorp, E.A.E. Ammar, J. Mater. Sci. 11 (1976) 1215–1219.
[12] J.H. Ryu, S.Y. Bang, J.W. Yoon, C.S. Lim, K.B. Shim, Appl. Surf. Sci. 253 (2007) 8408–8414.
[13] Q.L. Dai, H.W. Song, X. Bai, G.H. Pan, S.Z. Lu, T. Wang, X.G. Ren, H.F. Zhao, J. Phys. Chem. C 111 (2007) 7586–7592.
[14] M.V. Nazarov, D.Y. Jeon, J.H. Kang, E.J. Popovici, L.E. Muresan, M.V. Zamoryanskaya, B.S. Tsukerblat, Solid State Commun. 131 (2004) 307–311.
[15] K.W. Cho, J.H. Choi, S.W. Mhin, K.M. Kim, J.I. Lee, J.H. Ryu, J. Vac. Sci. Technol. B 33 (2015) 041201.
[16] Y.B. Xiang, J.M. Song, G. Hu, Y. Liu, Appl. Surf. Sci. 349 (2015) 374–379.
[17] Y.Y. Wang, J. Song, Y.R. Zhao, L. Xu, D.P. He, H. Jiao, Powder Technol. 275 (2015) 1–11.
[18] Y.F. Zhang, L.M. Wang, D.Q. Chu, H.M. Sun, A.X. Wang, Z.C. Ma, L.F. Yang, Y. Zhuang, Y.Z. Bai, CrystEngComm 17 (2015) 2444–2449.
[19] X.F. Wang, G.H. Peng, N. Li, Z.H. Liang, X. Wang, J.L. Wu, J. Alloys Compd. 599 (2014) 102–107.
[20] L. Lv, X.Q. Liu, C. Xu, X.J. Wang, J. Nanosci, Nanotech 14 (2014) 3521–3526.
[21] J.H. Kim, H.Y. Choi, E.O. Kim, H.M. Noh, B.K. Moon, J.H. Jeong, Opt. Mater. 38 (2014) 113–118.
[22] L. Costa, L. Rossi di Montelera, G. Camino, E.D. Weil, E.M. Pearce, Polym. Degrad. Stab. 56 (1997) 23–35.
[23] Y. Zhao, N. Yan, M.W. Feng, Thermochim. Acta 555 (2013) 46–52.
[24] V.S. Marques, L.S. Cavalcante, J.C. Sczancoski, A.F.P. Alcântara, M.O. Orlandi, E. Moraes, E. Longo, J.A. Varela, M.S. Li, M.R.M.C. Santos, Cryst. Growth Des. 10 (2010) 4752–4768.
[25] L.S. Cavalcante, V.M. Longo, J.C. Sczancoski, M.A.P. Almeida, A.A. Batista, J.A. Varela, M.O. Orlandi, E. Longo, M.S. Li, CrystEngComm 14 (2012) 853–868.
[26] A.K. Parchur, A.A. Ansari, B.P. Singh, T.N. Hasan, N.A. Syed, S.B. Rai, R.S. Ningthoujam, Integr. Biol. 6 (2014) 53–64.
[27] Maheshwary, B.P. Singh, J. Singh, R.A. Singh, RSC Adv. 4 (2014) 32605–32621.
[28] Y.S. Luo, X.J. Dai, W.D. Zhang, Y. Yang, C.Q. Sun, S.Y. Fu, Dalton Trans. 39 (2010) 2226–2231.
[29] Z.J. Luo, H.M. Li, H.M. Shu, K. Wang, J.X. Xia, Y.S. Yan, Cryst. Growth Des. 8 (2008) 2275–2281.
[30] A. Khanna, P.S. Dutta, J. Solid State Chem. 198 (2013) 93–100.
[31] L.L. Li, R.Q. Li, W.W. Zi, S.C. Gan, Phys. B 458 (2015) 8–17.